International Journal of Rock Mechanics & Mining Sciences 160 (2022) 105256

Contents lists available at ScienceDirect

International Journal of Rock Mechanics and Mining Sciences

journal homepage: www.elsevier.com/locate/ijrmms

# Experimental observations on the effect of strain rate on rock tensile fracturing

Mahmoud Alneasan [a], Mahmoud Behnia [a,*], Abdel Kareem Alzo'ubi [b]

[a] Department of Mining Engineering, Isfahan University of Technology (IUT), Isfahan, 8415683111, Iran
[b] Civil Engineering Department, Abu Dhabi University, Al Ain, United Arab Emirates

ARTICLE INFO

Keywords:
Tensile fracture
Strain rate
Crack propagation speed
Tortuosity
Fracture width

ABSTRACT

Tensile fracturing was investigated in this study under a static ($10^{-5}$) and quasi-static ($10^{-3}$ and $10^{-2}$ $S^{-1}$) strain rate in three different rock types (marlstone, marble, and hornfels). In addition, the effect of $\dot{\varepsilon}$ on the microscopic properties of the fracture such as the width and tortuosity was investigated by tracing the fracture path under the microscope. The results indicated that by increasing the $\dot{\varepsilon}$ from $10^{-5}$ to $10^{-2}$ $S^{-1}$, the crack propagation speed in marlstone and marble increased from 4 to 22 m/s and in hornfels from 35 to 100 m/s. The improvement of the parameters associated with hydraulic fracturing is achieved by reducing the $\dot{\varepsilon}$. By reducing the $\dot{\varepsilon}$ from $10^{-2}$ to $10^{-5}$ $S^{-1}$, the (fracture toughness, and breakdown pressure) in marlstone, marble, and hornfels decreased by (37%, 22%), (42%, 30%), (46%, 39%), respectively. In addition, the width of the fracture was strongly affected by the $\dot{\varepsilon}$, this parameter increased by 55%, 36%, and 51% in marlstone, marble, and hornfels, respectively, when the $\dot{\varepsilon}$ decreased from $10^{-2}$ to $10^{-5}$ $S^{-1}$. In the very fine- and fine-grained rocks such as marlstone and hornfels; by decreasing the $\dot{\varepsilon}$ from $10^{-2}$ to $10^{-5}$ $S^{-1}$, the tortuosity factor decreased only by about 0.4%, while in the medium- to coarse-grained rocks such as marble decreased by 4.6%.

## 1. Introduction

Rock mass contains many pre-existing cracks and flaws that can propagate under the effect of different loading patterns. Tensile fracturing is common in rock mechanics and the tensile cracks can be naturally found in the rock mass or can be artificially created for different purposes. For example, opening mode I tensile fractures are observed around dynamic shear ruptures such as in the extensional side of the normal fault in the Vaca Muerta formation, northwest Argentina.[1] In addition, folding can cause tension such as along the top of an anticlinal fold axis. Therefore, the tensile fracture can grow parallel to the fold axis. One of the most important applications of artificial tensile fractures is hydraulic fracturing which is commonly used to increase the productivity of oil and gas wells or to open geothermal reservoirs.

In general, artificial tensile fractures in a rock mass can be induced under different strain rates and this will affect the rock behavior significantly. The effect of strain rate on the rock behavior was investigated by many researchers. They focused on the effect of this parameter on the strength properties of rocks and they concluded that increasing the strain rate will increase both the rock strength[2–4] and fracture toughness.[5–7] In addition, analytical, numerical, and experimental models were developed to study tensile fracturing for mechanical, geological, and geophysical purposes.[8] Yoffe[9] presented an analytical model for a moving crack tip under pure tension by taking into account the effect of crack propagation speed. Yamashita[10] developed a numerical model to study tensile cracks around propagating shear ruptures. Numerical models were developed for tensile crack propagation in semi-circular,[11] Brazilian disk,[12,13] rectangular,[14,15] and other samples.[16] In the experimental field, Griffith, et al.[17] and Ngo et al.[18] investigated the creation of tensile cracks during propagating earthquake ruptures.

Hydraulic fracturing is one of the direct applications of tensile fracturing and has gained in popularity due to its importance in measuring in situ stresses or increasing the productivity of oil and gas wells. Many researchers have worked in this area to investigate the effect of different parameters on the conductivity and permeability of complex network fractures caused by this technology. Mighani et al.[19] investigated tensile fracturing of anisotropic rocks with its application in hydraulic fracturing and concluded that the resulting unpropped fractures increased the permeability by orders of magnitude. Zhang et al.[20,21] measured numerically the conductivity of unpropped and propped natural or hydraulic fractures in Barnett shale by taking the

* Corresponding author.
E-mail addresses: m.alneasan@mi.iut.ac.ir (M. Alneasan), behnia@cc.iut.ac.ir (M. Behnia), abdel.alzoubi@adu.ac.ae (A.K. Alzo'ubi).

https://doi.org/10.1016/j.ijrmms.2022.105256
Received 5 September 2021; Received in revised form 29 August 2022; Accepted 20 October 2022
Available online 12 November 2022

effect of water damage on the conductivity of shale fractures into account. Lu et al.[22] used granite and stainless-steel plates to develop an orthogonal fracture network model. They concluded that the increase inflow capability, the nonlinearity of the flow pattern, and the parallel fracture to the main fracture significantly increase the conductivity of the fracture network system. Zhao et al.[23] observed that brittle minerals in the matrix strongly affect the creation of fracture network.

For example, horizontal stress convergence, the presence of high brittle minerals, and the high value of horizontal elastic modulus are considered a favorable environment for the creation of fracture network. In addition, proppant transport and settling in complex hydraulic fracture system is important to keep new fractures open after stress releases.[24–26] Proppant can be distributed in tensile fractures caused by hydraulic fracturing to maintain open fractures with high productivity. Hydraulic fracturing can be conducted under different flow rates and as a consequence, tensile cracks can be induced in a rock mass under different strain rates. Therefore, studying the effect of strain rate on the microscopic characteristics of tensile fractures such as the fracture width and tortuosity is critical to understanding how can we reduce the tortuosity and increase the width of the fracture path in low, medium, and high-strength rocks. Hence, increasing the permeability and conductivity of these fractures. In addition, because the rock material is dependent on strain rate and the rock strength increases with increasing the strain rate, the tensile strength and fracture toughness that directly affects the breakdown pressure are important to be investigated under different strain rates to obtain the minimum breakdown pressure. In our previous work, we investigated the effect of mineralogical composition and grain size distribution on tensile fracturing in brittle rocks.[27] Experiments were conducted under the same static strain rate of $10^{-5}$ $S^{-1}$ in only strong rocks of granite and hornfels. This study aims to investigate the effect of strain rate on the fracture toughness, crack propagation speed, tortuosity of the fracture path, and the fracture width after stress releases in low, medium, and high-strength rocks. The results were discussed in terms of their impact on the permeability of tensile fractures and their special importance in the field of rock mechanics and geological engineering.

## 2. Mineralogical study

The mineralogical study is the starting point to understand the

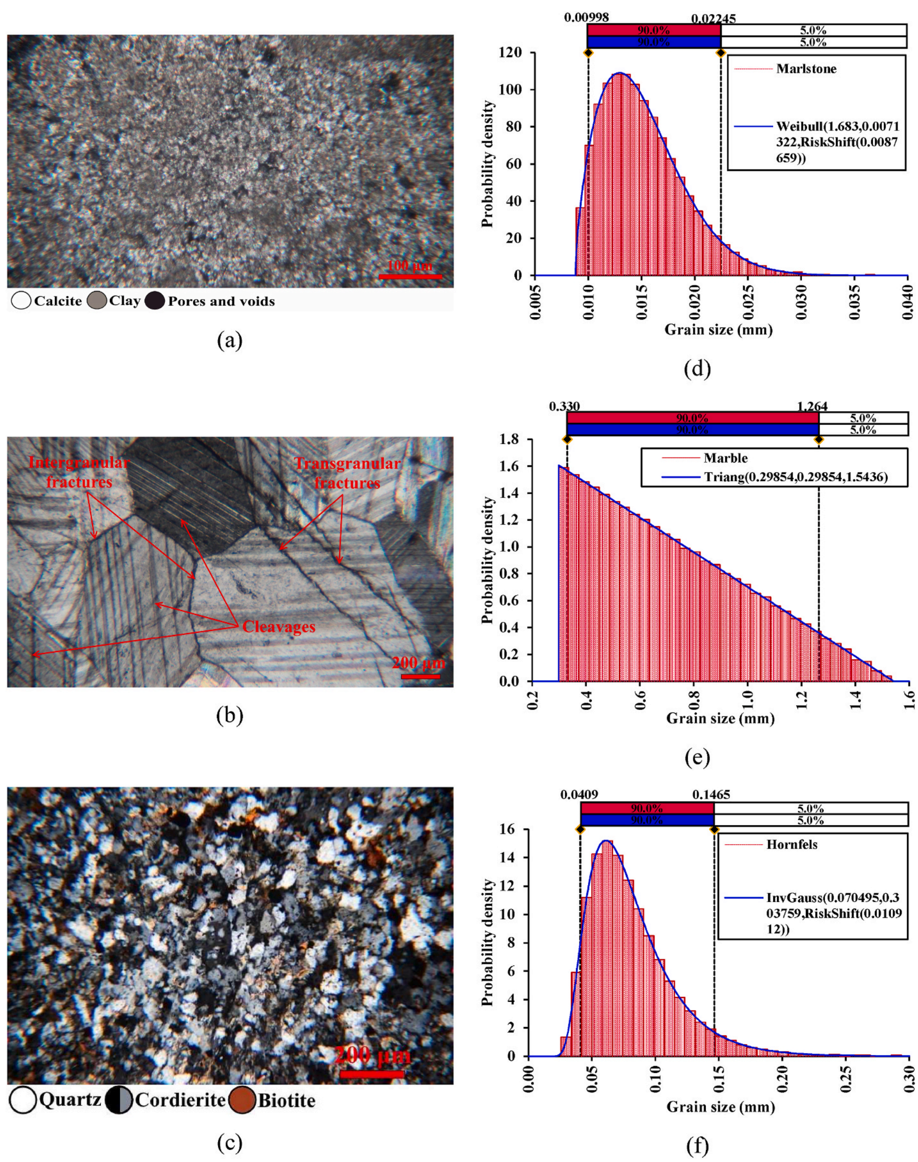


**Fig. 1.** (a, b, and c) Microscopic thin sections in marlstone, marble, and hornfels, respectively, (d, e, and f) grain size distribution in marlstone, marble, and hornfels, respectively.

composition of the rock samples in terms of grain types, sizes, and their impact on the final results. The rock materials used in this study are very fine-grained marlstone, fine-grained hornfels, and medium-to coarse-grained marble. Microscopic thin sections were taken to determine the mineralogical composition and grain size distribution of each rock type. Microscopic thins sections and grain size distribution for three rock types are shown in Fig. 1. The marlstone mainly consists of calcite (∼37%) and clay (∼63%) (Fig. 1-a). Therefore, this rock type is marly marlstone. Fig. 1-d shows that marlstone has grains with sizes between 0.01 and 0.02 mm and is classified as a very fine-grained rock because it has grain sizes less than 0.06 mm[28]. The high ratio of clay (63%) makes this rock weak, less brittle, and less permeable than marble and hornfels. In addition, the ratio of pores and voids in marlstone was about 6%. The main types of clay minerals in marlstone are shown in general based on the mineralogical composition observed by Shoval[29] in marl rocks, which are kaolinite, montmorillonite, illite, and mixed layers.

As for the marble, it mainly consists of crystalline calcite (∼100%). No other components were observed in the thin section of marble. The grain size distribution of marble (Fig. 1-e) shows that the predominant percentage (90%) is for grains of sizes between 0.33 and 1.3 mm and is classified as medium-to coarse-grained rock.[28] What distinguishes this rock from marlstone and hornfels is the presence of weak planes such as cleavages, and transgranular and intergranular fractures in the calcite grains. Intragranular microcracks can be found entirely in the calcite grains along cleavage planes. Moreover, intergranular fractures were observed along some boundaries of calcite grains. In addition, transgranular fractures that extend over more than one grain were also observed.

The third rock type is hornfels. The mineralogical composition of this rock type is the same as that of granite but this rock is stronger than granite.[27] Fig. 1-c shows that hornfels rock mainly consists of 53% cordierite, 26% quartz, and 21% biotite and is classified as a fine-grained rock because it has grain sizes between 0.06 and 0.2 mm[28] (Fig. 1-f).

Considering the mineralogical composition and grain size distribution of the three rock types, it can be noted that each of these rocks has a unique property that might have a special effect on the tensile fractures. Marlstone adds the effect of very fine grains on tensile fracturing, especially the effect of weak components such as clay. Marble takes the effect of natural fractures such as intragranular, intergranular cracks, and weak cleavages into account. While hornfels represents the effect of strong minerals on tensile fractures. Three types of rock; sedimentary (marlstone), metamorphic (marble), and igneous (hornfels) were investigated in this work. In addition, this study covers weak, medium, and high-strength rocks. Igneous and metamorphic rocks form good reservoirs for geothermal energy,[30–32] while sedimentary rocks such as marlstone can form part of oil reservoirs as mentioned by Cui et al.[33], FU et al.[34] Therefore, hydraulic fracturing might be performed in any of the three rock types selected in this work to increase the permeability and conductivity of working fluids (water or supercritical $CO_2$) in geothermal reservoirs, or to increase the productivity of oil and gas wells. In addition, hydraulic fracturing is frequently used to measure in-situ stresses at different depths. In this case, hydraulic fracturing can be performed in all rock types (sedimentary, metamorphic, and igneous) that have different strengths.

## 3. Physical and mechanical properties

The physical and mechanical properties of the three rock types were determined depending on established standards in rock mechanics (ISRM). Physical and mechanical properties include density, porosity, void ratio, moisture ratio, saturation ratio, tensile strength, sound wave velocities, Young's modulus, and Poisson's ratio see Table 1. The density of hornfels is 3% and 6% larger than the density of marble and marlstone, respectively. Marlstone has the lowest density and the highest porosity of the three rock types. Although natural fractures were observed in crystalline calcite in marble, this rock does not show high porosity. This is because these fractures are closed and they differ from the open pores and voids in marlstone.

According to the mechanical properties, the three rock types show a clear difference in the sound wave velocity and the dynamic young's modulus which were measured by using Proceq Pundit Lab + instrument for cylindrical specimens of the three rock types with (H/D = 2, NX dimensions). By changing the rock type from marlstone to marble and hornfels, the sound wave velocity increases. The dynamic Young's modulus of the hornfels, which was computed depending on the sound wave velocities, is greater than the dynamic Young's modulus of marble and marlstone. $E_{hornfels}$ is 1.9 and 2.8 times greater than $E_{marble}$ and $E_{marlstone}$, respectively. Moreover, the Poisson's ratio was computed depending on P and S wave velocities and it was found that the Poisson's ratio of marlstone is 0.28 and it is about 1.27 times the Poisson's ratio of marble and hornfels. By increasing the Poisson's ratio, the material behavior gradually transforms from brittle to ductile behavior. As mentioned previously, a high ratio of clay in marlstone makes this rock type less brittle and more ductile than others. This point is important in this study to take the effect of material brittleness on tensile fractures.

In addition, the three rock types can be classified depending on the Unconfined Compressive Strength (UCS) as shown by Bieniawski[35] and ISRM (1979) as follows: marlstone has low to moderate UCS between 10 and 30 MPa. Marble has UCS between 40 and 60 MPa and is classified as a medium-strength rock. Hornfels is classified as a high-strength rock because it has UCS greater than 200 MPa.

### 3.1. Brazilian splitting test

The Brazilian splitting test is the most common test to determine the tensile strength of rock materials. Brazilian tensile strength for the three rock types was determined depending on the ISRM suggested methods for determining the tensile strength of rock materials[36] for disk with dimension ($H/D = 0.5$, $H = 27$, and $D = 54$ mm) by using GOTECH AI-7000 LA testing machine. Displacement-load curves for the three rock types under the Brazilian tensile test are shown in Fig. 2. This figure shows that the peak load increases by changing the rock type from marlstone, to marble and hornfels. In addition, due to the high strength and brittleness of hornfels, this rock sustains more stress than marlstone and marble at less corresponding displacements.

Despite the simplicity of the Brazilian tensile test, this test can be used for other useful studies related to the tensile cracks induced by static and/or dynamic loads in rock samples, especially those studies related to hydraulic fracturing. The main difference between the Brazilian splitting test and hydraulic fracturing is in the mechanism of

**Table 1**
Physical and mechanical properties of the three rock types.

| Property type | Physical properties | | | | | Mechanical properties | | | | |
|---|---|---|---|---|---|---|---|---|---|---|
| Property | Density | Porosity | Void ratio | Moisture ratio | Saturation ratio | P-wave | S-wave | R-wave | Dynamic Young's modulus | Poisson's ratio |
| Symbol | $\rho$ | $n$ | $e$ | $w$ | $S_r$ | $C_p$ | $C_s$ | $C_r$ | $E_d$ | $\nu_d$ |
| Unit | $gr/cm^3$ | % | % | % | % | m/s | m/s | m/s | GPa | – |
| Marlstone | 2.63 | 11.2 | 12.6 | 2.14 | 49.3 | 3789 | 2095 | 1933 | 30 | 0.28 |
| Marble | 2.7 | 0.51 | 0.52 | 0.04 | 20 | 4377 | 2604 | 2378 | 45 | 0.23 |
| Hornfels | 2.77 | 0.23 | 0.23 | 0.02 | 28.6 | 5928 | 3545 | 3234 | 85 | 0.22 |

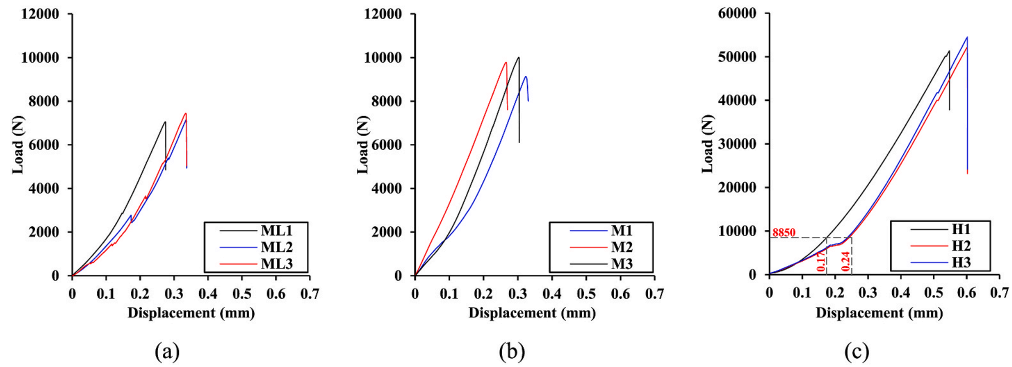


**Fig. 2.** Displacement-load curves for the three rock types under Brazilian tensile test, (a) marlstone, (b) marble, and (c) hornfels.

fracture initiation. Under hydraulic fracturing, the rock sample is subjected to internal fluid pressure. But under the Brazilian splitting test, the rock sample is subjected to external compressive stress at its two ends, which causes horizontal tensile stress along the vertical diameter. However, in both cases (hydraulic and Brazilian tests) the fracture occurs under tension stresses. Chen et al.[37] compared fracture surfaces induced by hydraulic fracturing and Brazilian splitting, they concluded that the tortuosity of the fracture path is a function of rock heterogeneity and is greater in the Brazilian splitting test than that in hydraulic fracturing. In this study, the Brazilian disks were examined after the test and found to have primary tensile fractures, minor shear fractures, and fractured shear zones in the three rock types as shown in Fig. 3. Analytically, the Brazilian disk is split into two equal semicircles after the test. This is a theoretical case and can happen in completely homogeneous and isotropic materials. But in rock materials, because these materials are heterogeneous and have different grain types and sizes as shown in Fig. 1, the primary tensile fracture is not straight and in rare cases, the rock sample is divided into two equal semicircles as in the back face of sample 2 of marlstone (Fig. 3). In addition, due to shear stress concentration between loading plates and rock samples, minor shear fractures are created near the loading plates. It can be noted that one primary tensile fracture with some fractured shear zones developed in the marlstone. Because marlstone is weaker and less brittle than marble and hornfels, the loading area is crushed due to shear stress concentration, and fractured shear zones are formed. In addition, the fracture path was enlarged and shown below in Fig. 3. As observed, the tensile fracture in marlstone is straighter and less tortuous than that in marble and hornfels. Because marble has the largest grain size and due to the effect of different defects in this rock type, fracture grows between and through rock grains and it becomes more tortuous than that in marlstone and hornfels. Therefore, it can be noted that the fracture path in marble is 5% and 7% greater than that in hornfels and marlstone, respectively.

In marble, one primary tensile fracture was created in all rock samples and fractured shear zones were noted in only one specimen (sample 2). An important point can be observed in this rock type which is the growth of two primary tensile fractures from the upper and lower surfaces of the rock sample. These two fractures coalesced near the specimen center. As shown in the lower right corner of Fig. 3, a tensile fractured zone is created due to the coalescence of two tensile fractures. The presence of such areas plays a major role in increasing the porosity and thus increasing the permeability of the fractured rocks.

In hornfels, more than one tensile fracture is created. This is due to the high strength and brittleness of this rock type. The peak load under Brazilian tests (Fig. 2) in hornfels is six and seven times greater than that in marble and marlstone, respectively. Therefore, a large amount of energy is stored in the hornfels rock before the creation of tensile cracks. This energy is dissipated inside the rock sample by forming more than one tensile fracture. As in the case of the blast, where the rock mass is exposed to large energy within a short time, this large energy is dissipated by the growth of a large number of radial tensile cracks in the damaged zone around the borehole. In addition, minor shear cracks are observed near the loading plates in hornfels. Comparison between low, medium, and high-strength rocks under the Brazilian splitting test, due to the ability of hornfels to store high energy before fracturing, more than one tensile fracture is created and the Brazilian disk is divided into three or more parts. While in low and medium-strength rocks such as marlstone and marble, one tensile fracture is created and the Brazilian disk is divided into two parts.

Brazilian tensile strength (BTS) is shown in Table 2. This table shows that the BTS of hornfels rock is 22.55 MPa and it is 5.6 and 7.6 times greater than that of marble and marlstone, respectively. Although marble is 100% calcite and this component is stronger than clay which forms 63% of marlstone, the BTS of marble is only a little larger than that of marlstone. This is due to the presence of weak surfaces and defects in this marble. Stress concentrates at the tips of preexisting defects and therefore, these defects grow and coalesce to form a primary tensile fracture.

## 4. Three points bending test

Fracture toughness was measured in this study by using the three points bending test in rectangular rock specimens. As shown in Fig. 4-a, under this test the rock sample rests on two bottoms supports with a span of 2S and is subjected to vertical load *P* which is aligned along the direction of the artificial notch. The dimensions of rectangular specimens were determined according to ASTM E399 – 12E3 standard and the study of Mousavi et al.[38] Because of the rock heterogeneity and for the reliability of the results, each test was repeated three times. In addition, to study the effect of strain rate on the fracture toughness and crack propagation path, our tests were conducted under three strain rates. Therefore, 9 rectangular rock samples were prepared from each rock type (Fig. 1-b).

Rectangular rock samples in this study were loaded by using the GOTECH AI-7000 LA testing machine. This machine has a capacity of 20 tons and the test speed can range between 0.001 and 250 mm/min. Taking into account the height of the rectangular specimen ($W = 50$ mm), the strain rate can change between $3 \times 10^{-7}$ and $8 \times 10^{-2}$ $S^{-1}$. Therefore, the static and quasi-static strain rates can be investigated by using the GOTECH machine. To study the effect of the static and quasi-static strain rate on the fracture toughness, fracture speed, and crack propagation path, three strain values of $1 \times 10^{-5}$, $5 \times 10^{-3}$, and $1 \times 10^{-2}$ $S^{-1}$ were chosen. Where the first strain rate is in the static range and the rest are in the quasi-static range. This is important to understand how rock behavior is affected by the static and quasi-static strain rates. Displacement-load curves under the three points bending test for three values of strain rates are shown in Fig. 5. This figure shows that by increasing the strain rate from $10^{-5}$ to $10^{-2}$, the average peak load in marlstone, marble, and hornfels increased by 1.73, 1.78, and two orders of magnitude, respectively. It can be noted that by increasing the rock

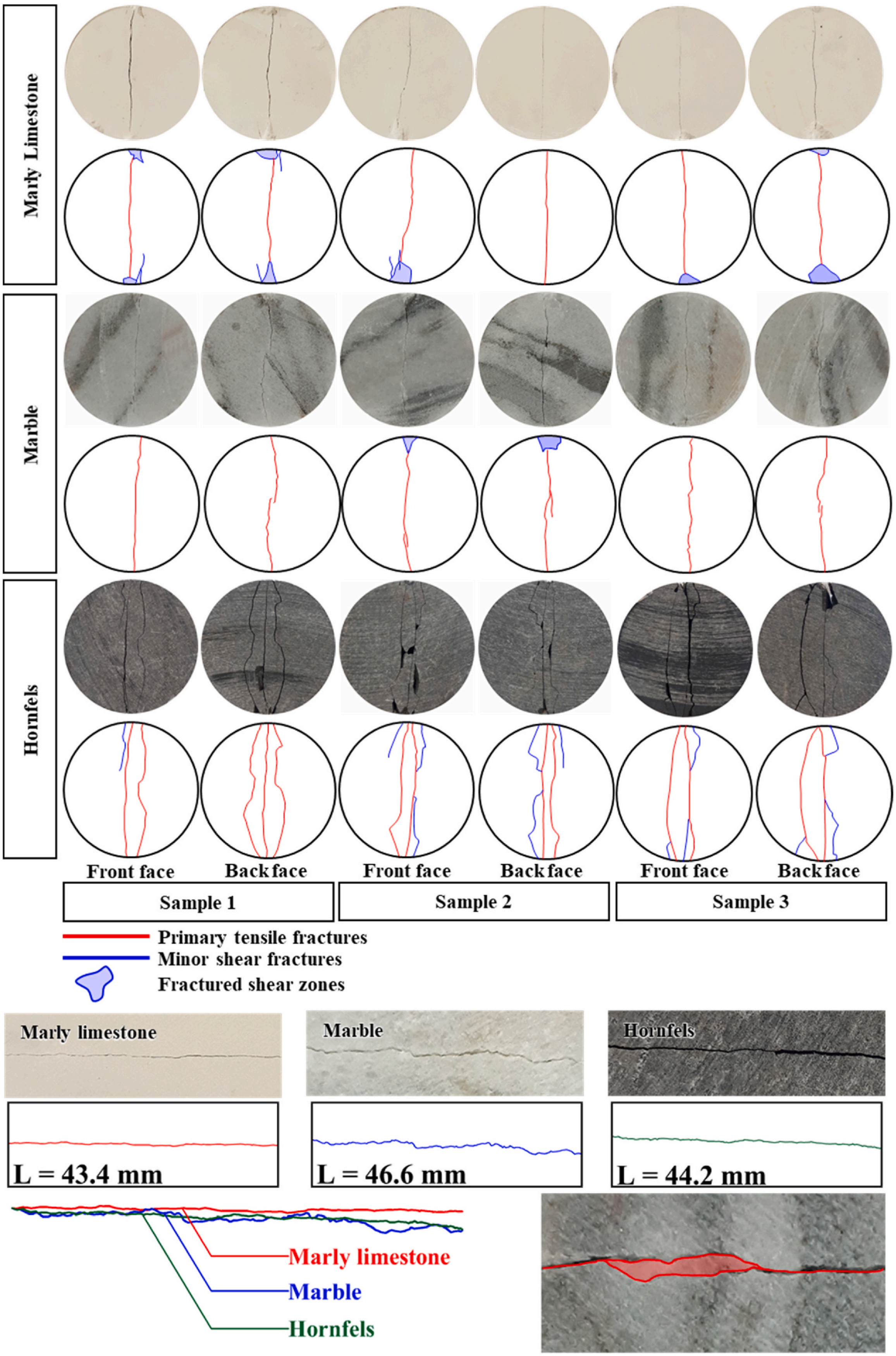


**Fig. 3.** Fracture patterns in the three rock types under the Brazilian tensile test.

**Table 2**
Brazilian tensile strength and fracture toughness under UBST and CRST.

| Rock type | BTS (MPa) | $K_{IC}$ under UBST | $K_{IC}$ under CRST | $\|\Delta K_{IC}\|$ |
|---|---|---|---|---|
| Marlstone | 2.95 ± 0.2 | 0.48 ± 0.07 | 0.65 ± 0.07 | 0.17 |
| Marble | 4.0 ± 0.25 | 0.55 ± 0.08 | 1.0 ± 0.02 | 0.45 |
| Hornfels | 22.55 ± 1.1 | 3.32 ± 0.16 | 2.01 ± 0.14 | 1.31 |

strength, the effect of strain rate increases.

In bounded rock mediums such as the rectangular specimens, stress and strain fields in the rock sample, stress intensity factors, and fracture toughness at the notch tip cannot be analytically obtained. Therefore, the rock sample should be simulated depending on numerical methods such as the Finite Element Method (FEM), Finite Difference Method (FDM), Boundary Element Method (BEM), etc. In this study, the rectangular rock sample was modeled depending on the BEM as shown in the next section.

### 4.1. Numerical simulation

To calculate stress intensity factors at the notch tip and fracture toughness in rectangular rock specimens under the three points bending test, the test was modeled by using the Displacement Discontinuity Method (DDM) which is a branch of the BEM. A numerical two-dimensional crack propagation code (TDCPC)[39–41] was used here to model the three points bending test. This code was verified by using the experimental and numerical results of other researchers. The rectangular specimen is firstly discretized into N DDM elements as shown in Fig. 6-a. The boundary conditions are defined by considering the loaded element at the center of the upper surface and two bottoms supports with a span of 2S at the lower surface. The loaded element is DDM element with normal stress $\sigma_n = P$ and the two bottom supports are defined as DDM elements with zero vertical displacements ($u_n = 0.0$). The number of other elements is (N-3) and they are free traction and have no boundary conditions. When running the TDCPC code, the load $P$

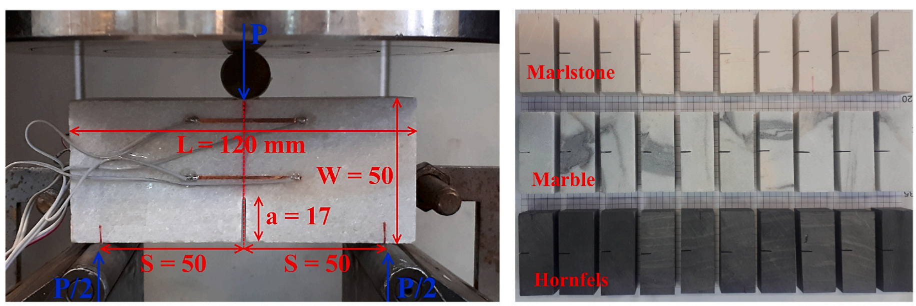


(a) (b)

**Fig. 4.** (a) Rectangular rock specimen under three points bending test, (b) 10 rectangular rock specimens of each rock type, all numbers are in millimeter.

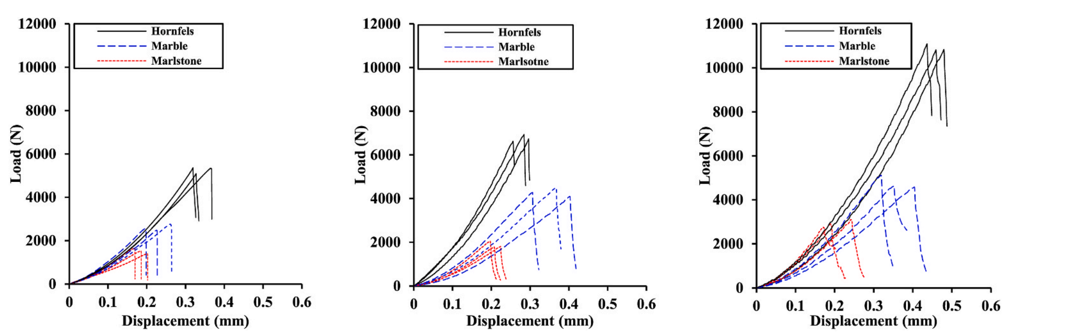


(a) (b) (c)

**Fig. 5.** (a) Displacement-load curves under three points bending test for a strain rate of (a) $1 \times 10^{-5}$, (b) $5 \times 10^{-3,}$ and (c) $1 \times 10^{-2}$

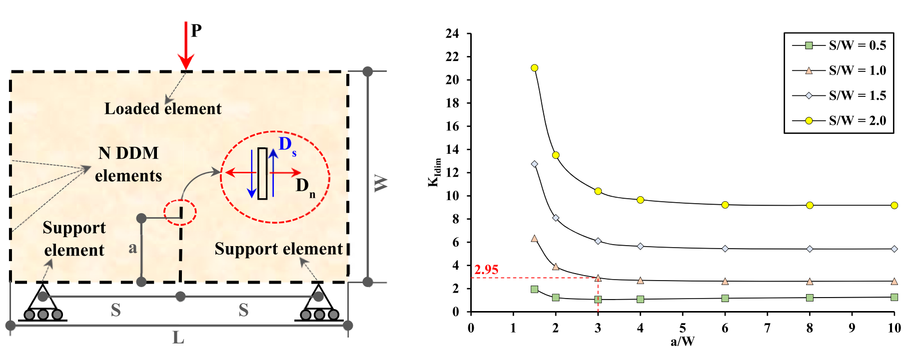


(a) (b)

**Fig. 6.** (a) Simulation of the three points bending test depending on DDM, (b) dimensionless stress intensity factor versus $a/W$ and $S/W$.

gradually increases from zero by small increments $\Delta P$, the normal and shear stresses induced by $P$, and the influence coefficients are calculated in all DDM elements. Influence coefficients are mainly a function of the geometry of each element and the elastic properties of the material. These coefficients link between the boundary conditions vector (B) and the displacement discontinuity vector ($D_n$ and $D_s$). Finally, a system of algebraic equations is formed, and by solving this system, $D_n$ and $D_s$ are calculated for each DDM element (equation (1)).

$$\left.\begin{aligned} B_s^i &= \sum_{j=1}^{N} A_{ss}^{ij} D_s^j + \sum_{j=1}^{N} A_{sn}^{ij} D_n^j \\ B_n^i &= \sum_{j=1}^{N} A_{ns}^{ij} D_s^j + \sum_{j=1}^{N} A_{nn}^{ij} D_n^j \end{aligned}\right\} i = 1 \text{ to } N \tag{1}$$

The most important element here is the crack tip element which is shown in the dashed circle in Fig. 6-a. Stress intensity factors ($K_I$ and $K_{II}$) are calculated as follows[42]:

$$KI = \frac{G}{4(1-\nu)}\sqrt{\frac{2\pi}{a_t}} D_{n,a} K_{II} = \frac{G}{4(1-\nu)}\sqrt{\frac{2\pi}{a_t}} D_{s,a} \tag{2}$$

in which $G$ and $\nu$ are shear modulus and Poisson's ratio, respectively, $a_t$ is the half-length of the crack tip element, $D_{n,a,}$ and $D_{s,a}$ are normal and shear displacement discontinuities at the crack tip element.

Under three points bending test, the notch tip is subjected to pure tensile stress, and therefore, $K_I \neq 0.0$ and $K_{II}$ should be zero. Otherwise, there is a problem with the model. When the external load $P$ reaches the peak load $P_{cr}$ that is experimentally determined, the fracture toughness ($K_{IC}$) can be calculated, which is equal to $K_I$ under ($P = P_{cr}$). Depending on the TDCPC, we present the following equation for calculating fracture toughness under the three points bending test in rectangular specimens:

$$K_{IC} = \frac{P_{cr}}{W.B} K_{I,dim}\sqrt{\pi a} \tag{3}$$

where $W$, $B$, and $a$ are the height, thickness, and notch length of the rectangular specimen, respectively. $K_{I,dim} = \sigma/\sqrt{(\pi a_t)}$ is the dimensionless stress intensity factor and is calculated numerically depending on the TDCPC. $K_{I,dim}$ is shown in Fig. 6-b for different values of $S/W$ and $a/W$. In this study $S/W = 1$ and $a/W = 0.3$, therefore, $K_{I,dim} = 2.95$.

### 4.2. Fracture toughness

Fracture toughness is an important property in mechanical engineering to determine the condition of crack propagation from a preexisting crack tip. Under the effect of external loads, stress concentrates at the tips of preexisting cracks. When the stress intensity factor reaches the fracture toughness of the material, these new cracks will initiate and coalesce with each other or stop before that. In this study, two methods were used to calculate fracture toughness. The first method is indirect and depends on the uncracked Brazilian splitting test (UBST) that was used to measure tensile strength in section 3.1. The second method depends on the results of cracked rectangular specimens under the three points bending test (CRST). The main difference between UBST and CRST is the presence of an artificial notch in the CRST. The fracture in the CRST grows due to stress concentration at the notch tip. When the tensile stress at the notch tip reaches tensile strength or in other words, when the $K_I$ attains the $K_{IC}$, the notch begins to grow. Under UBST there is no artificial notch and the fracture develops due to stress concentration at the tips of preexisting flaws which are naturally distributed in the rock material. Actually, natural preexisting cracks/flaws exist as well in the rectangular specimens, but because stress concentration at the notch tip is greater than that at any point in the rock sample and the notch is an open joint fracture begins to develop from the notch tip due to the high-stress concentration at the notch tip.[43] Fracture toughness under UBST can be calculated depending on the following equations:

$$K_{IC} = \frac{2P_{cr}}{\pi^{\frac{3}{2}} R^{\frac{1}{2}} T \alpha} f\left(\frac{a_{cr}}{R}\right) \tag{4}$$

$$f\left(\frac{a_{cr}}{R}\right) = \sqrt{\frac{a_{cr}}{R}} \int_0^{a_{cr}} \frac{g\left(\frac{r}{R}\right)}{\sqrt{a_{cr}^2 - r^2}} dr \tag{5}$$

$$g\left(\frac{r}{R}\right) = \frac{\left(1-\left(\frac{r}{R}\right)^2\right)\sin 2\alpha}{1 - 2\left(\frac{r}{R}\right)^2 \cos 2\alpha + \left(\frac{r}{R}\right)^4} - \arctan\left[\frac{1+\left(\frac{r}{R}\right)^2}{1-\left(\frac{r}{R}\right)^2}\tan\alpha\right] \tag{6}$$

For brittle material, $P_{cr}$ is the peak load and can be determined depending on Fig. 2, $R = 27$ mm is the radius of the Brazilian disk, $\alpha = 3^o$ is the half loading angel, $T = 27$ mm is the specimen thickness, $r$ is the radial distance from the center, $a_{cr}$ in eq. (4) is the critical crack length which corresponds to $P_{cr}$. In general, $a_{cr}$ is about 0.8 R[44]. Fracture toughness under CRST was computed depending on equation (3) and TDCPC. Fracture toughness under CRST with a linear fit and 95% confidence bars versus strain rate is shown in Fig. 7. This figure shows that the fracture toughness in the three rock types is strain rate dependent and it increases with increasing the strain rate. By increasing the strain rate from $10^{-5}$ to $10^{-2}$, the average value of $K_{IC}$ in marlstone, marble, and hornfels increases from 0.65 to 1.03, 1.0 to 1.72, and 2.01–3.73 MPa $m^{0.5}$, respectively. In addition, hornfels has the maximum fracture toughness, then marble and then marlstone. Moreover, the increment rate of $K_{IC}$ (the slope of linear fit) depends on the rock strength. The increment rate of marlstone, marble, and hornfels is 0.4%, 0.75%, and 1.8%, respectively. Therefore, the fracture toughness in strong rocks such as hornfels is more affected by the strain rate. This point is very important for design and research purposes. The strain rate levels under the effect of external loads should be determined and accordingly, an appropriate loading speed must be established for laboratory experiments.

Brazilian splitting tests were conducted under a strain rate of $10^{-5}$ $S^{-1}$. Therefore, the results of different experiments (UBST and CRST) should be compared under the same strain rate which is $10^{-5}$ $S^{-1}$. Fracture toughness under UBST was computed depending on equation (4) and they are shown in Table 2 with their counterparts under CRST.

For marlstone and marble, $K_{IC}$ under UBST is less than that under CRST. This indicates that the effect of preexisting natural flaws and voids in Brazilian disks of marlstone and marble on fracture toughness is greater than the effect of the artificial notch in rectangular specimens. According to microscopic sections in Fig. 1 and physical properties in

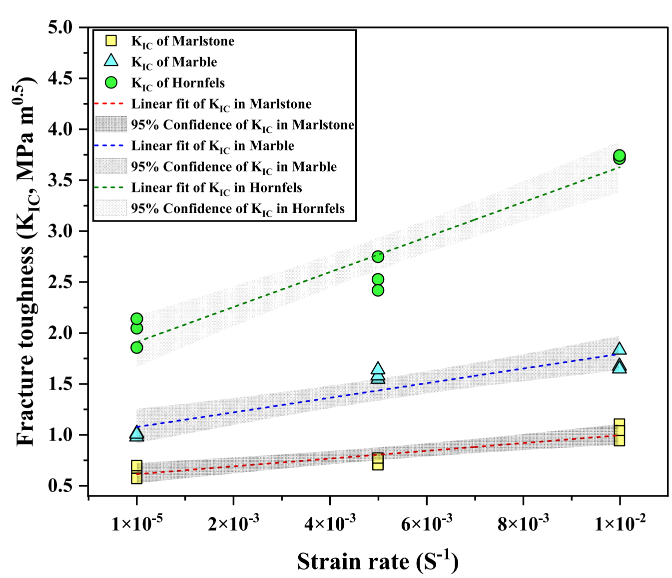


**Fig. 7.** (a) Fracture toughness under CRST versus strain rate.

Table 1, marlstone has the maximum porosity due to the high ratio of pores and voids that was observed in the microscopic section, and marble has different types of weak surfaces and defects. Depending on $\Delta K_{IC}$, it can be concluded that the effect of natural defects on the fracture toughness in the marble is greater than the effect of pores and voids in marlstone. In addition, Table 2 shows that in hornfels, $K_{IC}$ computed under UBST is greater than that under CRST. Hornfels has the minimum porosity ratio (0.23%) and no natural defects were observed under the microscope, therefore, the effect of the artificial notch in rectangular specimens of hornfels on fracture toughness was greater than the effect of natural pores and defects in Brazilian disks.

## 5. Crack propagation speed

The Crack propagation speed is an important parameter in analyzing quasi-static and dynamic problems. Under pure mode I, Broberg[45] indicated that the maximum crack propagation speed in brittle materials such as rocks is the Rayleigh wave speed. For a crack propagation speed, of less than 0.2 of the Rayleigh wave speed, the effect of crack propagation speed on stress and strain fields around the crack tip is very little and can be neglected. But for crack propagation speed greater than 0.2 of the Rayleigh wave speed, Freund[46] indicated that by increasing the crack propagation speed, stress and strain at the vicinity of the crack tip increase and they directly affect the preferred direction of the new branch. In addition, Yoffe[9] showed depending on the maximum tangential stress criterion that when the crack propagation speed under pure mode I exceeds a critical value ($0.68C_r$ for $\nu = 0.25$), a crack can grow through two branches instead of one branch. This is because by increasing the crack propagation speed, the stored energy at the crack tip increases, and this energy is dissipated by growing more than one branch from the crack tip. Based on the above, crack propagation speed is an important parameter in this study to understand how this parameter can be affected by changing the rock strength and strain rate. The crack propagation speed is one of the most difficult parameters to be experimentally measured, especially since it requires special and expensive equipment. An electrical circuit was previously developed[27,39] to measure the crack propagation speed in semi-circular specimens. This circuit mainly includes conductive copper tapes, power supplies, and a digital oscilloscope (Fig. 8-a).

The surfaces of the rock sample must be well polished to ensure complete contact between copper tapes and sample surfaces. Copper tapes are affixed to the front and back surfaces so that we can measure the crack propagation speed on two surfaces. When the notch begins to grow, the new crack cuts the first and second tapes, respectively. The cut-off time can be determined by a digital oscilloscope as shown in Fig. 8-b. For the front surface, copper tapes are connected to channels 1 and 2 in the oscilloscope and for the back surface, copper tapes are connected to channels 3 and 4. The crack propagation speed can be calculated depending on the time required for the crack to grow between two successive tapes and the length of the new fracture. The long memory of the oscilloscope used in this study is 1 M points/channel and the maximum sample rate of each channel is 2 GS/S. The record time was set to 2 s. Therefore, the signal is displayed from −1 to +1. Based on that, the sample rate for each channel is calculated by dividing the long memory by the record time, which is 1 M/2S = 500K points/S for each channel.

Crack propagation speed versus strain in the three rock types with a linear fit and 95% confidence bars are shown in Fig. 9. By increasing the strain rate from $10^{-5}$ to $10^{-2}$ $S^{-1}$, the crack propagation speed in marlstone and marble increases from 4 to 22 m/s, and in hornfels increases from 35 to about 100 m/s. Although marble is stronger than marlstone, they almost have the same crack propagation speed. In addition, hornfels has the maximum increment rate of crack propagation speed (65%), while marlstone and marble have the same increment rate of 18%. As will be shown later in section 6, due to the large grain size in marble and the presence of natural weak surfaces, the crack changes its path several times in a zigzag fashion, which makes it more tortuous and longer than that in marlstone. Changing the path direction leads to a loss of stored energy at the crack tip, and therefore the crack propagation speed in marble decreases.

Because marlstone and marble are weaker and less brittle than

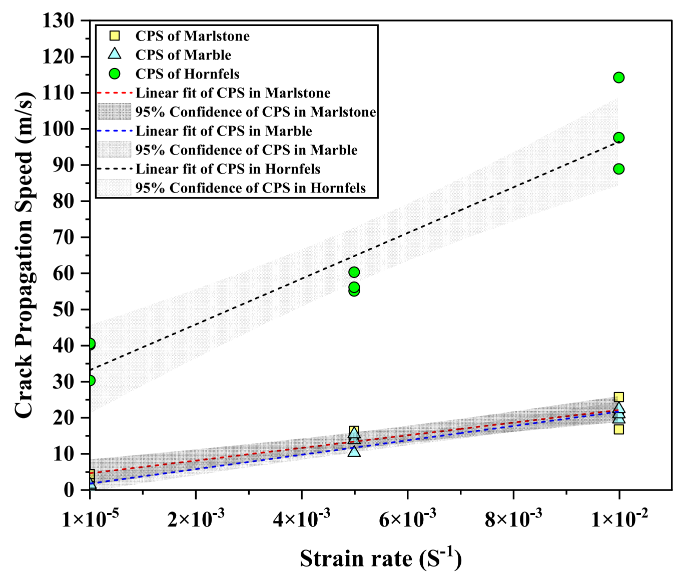


**Fig. 9.** Crack propagation speed versus strain rate in the three rock types.

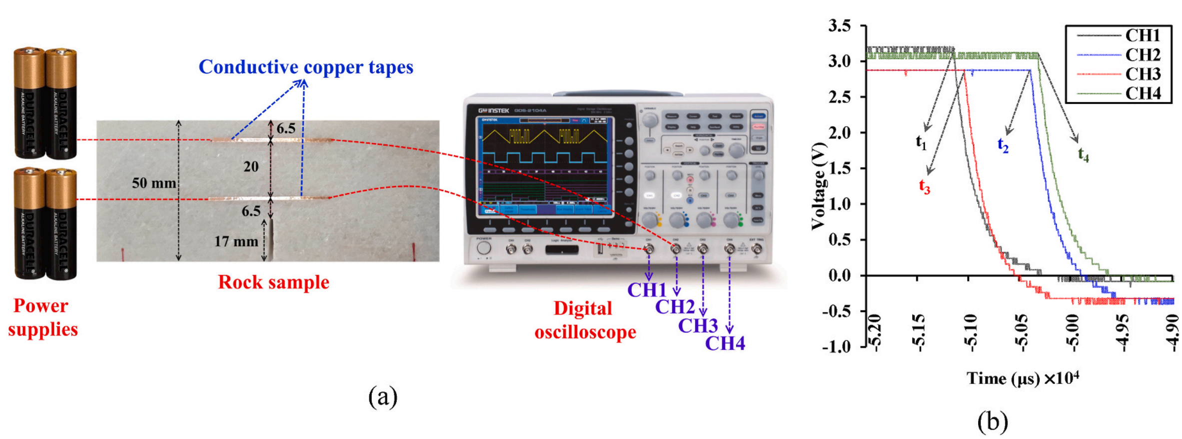


**Fig. 8.** (a) Electrical circuit for measuring crack propagation speed, (b) the signal captured by the oscilloscope.

hornfels, by increasing the external load *P*, small amounts of energy are stored at the crack tip and are gradually consumed as the crack grows over a relatively long period. But in hornfels, because this rock type is very strong, a large amount of energy is stored at the notch tip before it begins to grow, when the tensile stress reaches the tensile strength of the material, the stored energy is quickly released within a short period, which results in a large propagation speed.

## 6. Fracture path analysis

As it is known, rocks have a wide range of grain types and sizes. This issue greatly affects the results of this study, especially when compared to the analytical models used in linear elastic fracture mechanics. Fracture path analysis helps to understand how the fracture grows between different grain types and sizes. In addition, determining the fracture width after stress releases is important to measure the permeability of tensile fractures. This is important to study the effect of grain size distribution on the productivity of oil and gas wells in different rock types. Moreover, because in hydraulic fracturing the fluid can be injected at different rates, the strain rate around the borehole is a function of the injection rate, and therefore, the width of new tensile cracks can be affected by the injection rate that will be used to fracture the rock. Therefore, to investigate the effect of grain type, grain size distribution, and strain rate on the fracture path of tensile cracks, two microscopic thin sections were taken from each rock type under a strain rate of $10^{-5}$ and $10^{-2}$ as shown in Fig. 10. Successive pictures were taken by tracing the fracture path under a microscope. Then these pictures were combined using Photoshop without affecting the scale as shown in Fig. 11.

Analytically, under three points bending test in full homogeneous and isotropic materials, the crack grows in a straight line from the notch tip to the loaded point. This straight line is the path of the maximum tangential stress criterion. In the rocks, due to the heterogeneity and different grain sizes, the fracture grows across or between the grains and deviates from its straight path. When the fracture grows across the grains, the grain will split into two equal or unequal parts and an intragranular fracture is formed. The fracture toughness here mainly depends on the strength of the grains. When the fracture grows along the grain boundary, an intergranular fracture is formed and the fracture toughness is determined depending on the bonds strength between the grains. Due to very fine- and fine-grains in marlstone and hornfels, the number of intragranular and intergranular fractures cannot be counted. But in general, it was observed that intergranular fractures are predominant. In marble, due to the large grain size, intragranular and intergranular fractures can be easily distinguished. Intragranular fractures through the grains were marked with a red circle as shown in Fig. 11-c and Fig. 11-d. Under a strain rate of $10^{-5}$ (Fig. 11-c), the number of total fractures is 30, with 10 intragranular and 20 intergranular fractures. While under a strain rate of $10^{-2}$ (Fig. 11-d), the number of total fractures is about 35, with 12 intragranular and 23 intergranular fractures. It can be noted that under a low and high strain rate, the ratio of intragranular to intergranular fractures is the same and equals 0.5.

### 6.1. Tortuosity

To analyze the effect of the grain size on the straightness of the fracture path, a tortuosity factor ($\tau$) was computed. This factor was defined as the square of the ratio between the actual and the nominal length of the fracture path $(L_{act}/L_{nom})^2$ [47]. This factor shows how much the actual length is greater than the nominal length. In general, because the fracture path in rock materials is tortuous, the actual length is greater than the nominal length and the tortuosity factor is greater than one. The minimum value of the tortuosity factor is one, which means that the actual length is equal to the nominal length (theoretical case). By increasing this factor, the tortuosity of the fracture path increases and the straightness decreases. The results of this study showed that marlstone which has the finer grain size has the minimum tortuosity factor. By increasing the grain size, the tortuosity factor increases and it is the maximum for marble which has the largest grain size. Under a strain rate of $10^{-5}$, the tortuosity factor of the marble is 7.5% and 4.5% greater than that in marlstone and hornfels, respectively. In addition, it was observed that in the three rock types by increasing the strain rate, the tortuosity factor increases, especially in marble. Therefore, the straightness of the fracture path decreases by increasing the strain rate. The tortuosity factor in marlstone, marble, and hornfels increased by 0.5%, 4.8%, and 0.3% when the strain rate increased from $10^{-5}$ to $10^{-2}$ $S^{-1}$, respectively. Moreover, the effect of the strain rate on the tortuosity of the fracture path in medium-to coarse-grained rocks such as marble is greater than that in the very fine- and fine-grained rocks such as marlstone and hornfels.

### 6.2. Fracture width

As mentioned previously, fracture width ($W$) is the most important parameter here for analyzing the permeability and productivity of tensile cracks induced by hydraulic fracturing. To accurately analyze this parameter, the fracture width was measured every 0.1 mm along the fracture path, and the distribution of this parameter is shown on the right of Fig. 11. Considering the range between $W_{min}$ and $W_{max}$ and the averaged value $W_{av}$, fracture width in the three rock types versus the strain rate is shown in Fig. 12. This figure shows that the fracture width increases with increasing the grain size. Under a strain rate of $10^{-5}$, the $W_{av}$ in marble is 23% and 14% greater than that in marlstone and hornfels. While under a strain rate of $10^{-2}$, the $W_{av}$ in marble is close to that in hornfels, and it is 26% larger than that in marlstone. In addition, Fig. 12 indicates that the fracture width depends on the strain rate. By increasing the strain rate from $10^{-5}$ to $10^{-2}$ in marlstone, marble, and hornfels, the fracture width decreases by 36%, 26%, and 34%, respectively.

## 7. Discussion

Tensile fracturing is a crucial process for predicting crack initiation and propagation in reservoirs, and for generating new tensile cracks in hydraulic fracturing. The tensile strength is an important parameter that controls the opening and propagation of tensile cracks induced in rock masses.[48,49] Therefore, tensile fracturing was investigated in this study

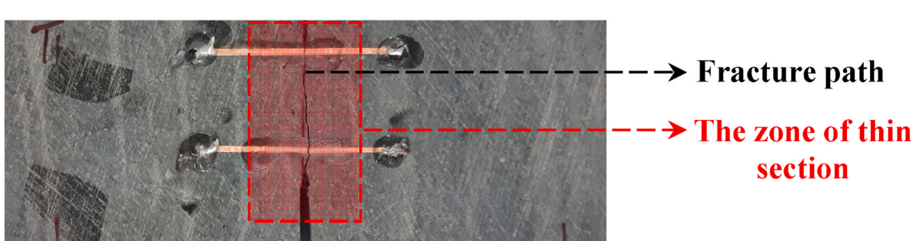


**Fig. 10.** The zone of a microscopic thin section from rectangular rock samples after test.

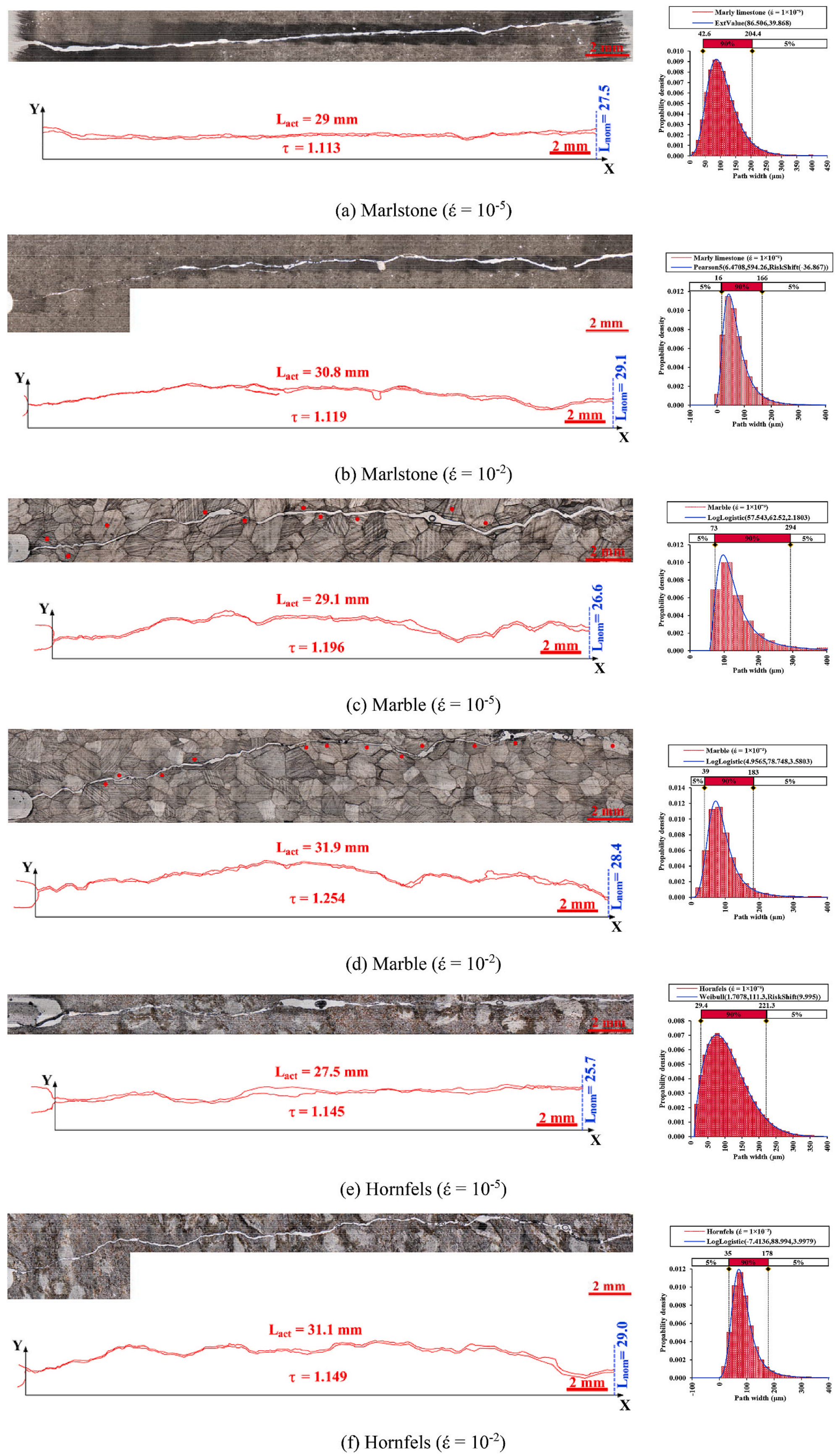


**Fig. 11.** Fracture path analysis in (a) marlstone ($\acute{\varepsilon} = 10^{-5}$), (b) marlstone ($\acute{\varepsilon} = 10^{-2}$), (c) marble ($\acute{\varepsilon} = 10^{-5}$), (d) marble ($\acute{\varepsilon} = 10^{-2}$), (e) hornfels ($\acute{\varepsilon} = 10^{-5}$), (f) hornfels ($\acute{\varepsilon} = 10^{-2}$).

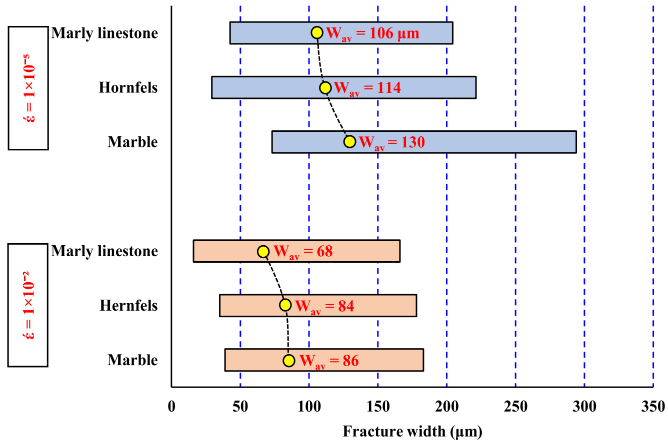


**Fig. 12.** Fracture width in the three rock types versus strain rate.

on a laboratory scale to show the effect of the strain rate on fracture toughness, crack propagation speed, the tortuosity, and width of the fracture path, to show the direct effect of these parameters on hydraulic fracturing in low, medium and high strength rocks.

### *7.1. Mineralogical composition and fracture speed*

In this work, we used three types of rocks; low strength marlstone, medium strength marble, and high-strength hornfels. Marlstone is characterized by very fine grain size (0.01–0.02 mm), high clay content (~63%), and the presence of voids and pores that increase its porosity. The most controlling factor in this rock type is the high clay content. Zhang et al.[50] investigated the effect of the textural and mineralogical components on the tensile strength of shale samples and concluded that the distribution and/or the number of clay minerals and the textures of the rock may be the most influential factor on the tensile strength. Moreover, the presence of clay minerals weakens the bond between the grains. For this reason, the experiments in this study show that marlstone has the lowest tensile strength and fracture toughness of all three types. In the case of marble which is characterized by a medium-to the coarse-grain size of calcite (0.33–1.3 mm) and the presence of different weak surfaces such as cleavages, we observed intergranular and intragranular fractures. Because the ends of these fractures are stress concentrators, the tensile strength and the crack propagation path are directly affected by the presence of such fractures. Therefore, the tensile strength in marble is a little greater than that in marlstone and the crack propagation speed is almost equal for both. The third rock type is hornfels, this rock represents the strong rock in this study and consists of strong minerals once compared with marlstone and marble. Due to the high strength of this rock type, it can store a large amount of energy before releasing it to create fractures, then this rock dissipates energy by creating more than one fracture as shown in Fig. 3. Although this rock was tested under a static and quasi-static strain rate, the rapid dissipation of stored energy at the moment of fracturing, compared to marlstone and marble, can cause a dynamic effect and this is one of the main differences between low, medium, and high strength rocks. In low and medium-strength rocks such as marlstone and marble, the energy is gradually stored and dissipated by generating new fractures, Table 1 shows that hornfels has a higher modulus of elasticity than marlstone and marble. Hence the importance of the amount of stored energy and crack propagation speeds in rocks. For example, under the same strain rate of $10^{-5}$ $S^{-1}$, the average crack propagation speed in marlstone and marble is 4 m/s and in hornfels is 35 m/s. Taking into account that the distance between every two conductive tapes is 20 mm (Fig. 8), the stored energy dissipated during 5000 µs in marlstone and marble and 571 µs in hornfels when the fracture grows from the lower to upper tape. By increasing the strain rate to $10^{-2}$ $S^{-1}$, the crack propagation speed in marlstone and marble increased to 22 m/s and in hornfels reached 100 m/s, therefore, the time required for energy dissipation in marlstone and marble is 909 µs and in hornfels is 200 µs. Consequently, when the strain rate increases from $10^{-5}$ to $10^{-2}$ $S^{-1}$, the required time for energy dissipation for fracture propagation along 20 mm decreased by 82% in marlstone and marble and by 65% in hornfels, one of the main reasons is the difference in the stiffness between these rock types.

### *7.2. Fracture toughens and breakdown pressure*

The strain rate has also a major effect on the fracture toughness; by increasing the strain rate from $10^{-5}$ to $10^{-2}$ $S^{-1}$, the fracture toughness in marlstone, marble, and hornfels increased from 0.65 to 1.03, 1.0 to 1.72, and 2.01–3.73 MPa $m^{0.5}$, respectively. Johnson et al.[51] introduced the following equation to compute the breakdown pressure as a function of the fracture toughness for a cracked borehole.

$$P_b = [1 - I(\beta)]\sigma_h + I(\beta)\sigma_H + \frac{K_{IC}}{f(a/R)\sqrt{\pi a}} \tag{7}$$

where $\sigma_h$ and $\sigma_H$ are the minimum and maximum horizontal stresses, respectively; $I(\beta)$ is a function of the angle $\beta$ between the $\sigma_H$ and the crack with a length of $a$; $R$ is the radius of the borehole and $f(a/R)$ was shown by Paris, Sih[52] as a function of $a/R$. As shown in eq. (7), the breakdown pressure is directly proportional to the $\sigma_h$, $\sigma_H$, and $K_{IC}$ and inversely proportional to the crack length $a$. To show the effect of the strain rate on the Pb, the following parameters were chosen as shown by Mohamadi et al.[53]: $\sigma_h = 5.1$ MPa, $\sigma_H = 12.8$ MPa, $\beta = 0.0^o$, $I(\beta) = -0.058$, $a = 1.4$ mm, $R = 56$ mm and $f(a/R) = 2.21$. The breakdown pressure is shown in Table 3. This table shows that as the strain rate increases the breakdown pressure increases. This result was confirmed by researchers in granite,[54] clay shale,[55] and cement and mortar,[56] who demonstrated an increase in breakdown pressure with increasing the injection rate. In hydraulic fracturing, we aim to reduce the breakdown pressure. Our results indicated that this can be done by decreasing the strain rate. Table 3 shows that by decreasing the strain rate from $10^{-2}$ to $10^{-5}$ $S^{-1}$, the ($K_{IC}$, $P_b$) in marlstone, marble, and hornfels decreased from 37% to 22%, 42%–30%), and 46%–39%, respectively. In addition, it can be noted that the effect of the strain rate on breakdown pressures increases with increasing the rock strength. Therefore, to reduce the breakdown pressure, it is recommended to reduce the injection rate in hydraulic tests. However, there is an important point that must be considered, which is that water infiltration is closely related to the injection rate (q), there is a minimum injection rate ($q_{min}$) under which the injection fluid penetrates inside the rock with constant injection pressure. This corresponds to an impermeable case and the injection rate must be increased to reopen the existing fractures or to create new tensile fractures. Therefore, in future works, we recommend studying the strain rate ($\dot{\varepsilon}_{min}$) corresponding to the minimum injection rate ($q_{min}$).

### *7.3. The tortuosity and fracture width*

In addition to what was mentioned above, studying the factors that affect the permeability and conductivity properties of tensile fractures is important in many fields of rock mechanics and geological engineering, and has practical applications such as the development of geothermal

**Table 3**
Breakdown pressure.

| Rock type | Strain rate ($S^{-1}$) | $K_{IC}$ (MPa $m^{0.5}$) | KIC-decrease (%) | $P_b$ (MPa) | Pb-decrease (%) |
|---|---|---|---|---|---|
| Marlstone | $10^{-2}$ | 1.03 | 37% | 11.7 | 22% |
| | $10^{-5}$ | 0.65 | | 9.1 | |
| Marble | $10^{-2}$ | 1.72 | 42% | 16.4 | 30% |
| | $10^{-5}$ | 1 | | 11.5 | |
| Hornfels | $10^{-2}$ | 3.73 | 46% | 30.1 | 39% |
| | $10^{-5}$ | 2.01 | | 18.4 | |

energy, the isolation of nuclear wastes buried in geological formations, drilling fluids flow during oil exploration operations, the recovery of fossil fuels, oil and gas flow through tensile fractures induced by hydraulic fracturing. In this study the effect of the strain rate on two factors that affect the permeability of tensile fractures was studied under a microscopic scale, these factors are the tortuosity and the aperture of the fracture path. Tortuosity is an essential factor that affects the connectivity of fluid flow paths because of contact areas along the fracture path.[57] Lespinasse, Sausse[58] indicated that the tortuosity and the fracture roughness strongly affect the fluid flow through fractures. The increase of fracture tortuosity causes an increase in the curved fractures along the fracture path, which in turn increases the friction between the proppant and fracture surfaces. In hydraulic fracturing, we strive to reduce the fracture tortuosity to reduce frictions in proppant transport and thus increase fracture productivity. The results of this study indicated that this can be achieved by reducing the strain rate. The tortuosity factor in the very fine- and fine-grained rocks such as marlstone and hornfels is affected slightly by the strain rate. By decreasing the strain rate from $10^{-2}$ to $10^{-5}$ $S^{-1}$, the tortuosity factor decreased only by 0.5% and 0.3% respectively. While in coarse-grained marble, the tortuosity factor decreased by 4.6%.

The second important factor that affects the fracture permeability is the aperture, or in other words the opening size, of the fracture path after stress releases. Our results indicated that the fracture width is more affected by the strain rate than the tortuosity factor. By decreasing the strain rate from $10^{-2}$ to $10^{-5}$ $S^{-1}$, the fracture width increased by 55%, 36%, and 51% in marlstone, marble, and hornfels, respectively. Therefore, the increase in strain rate decreases the fracture productivity because it decreases the fracture aperture. Finally, it can be concluded that the strain rate has a strong effect on the parameters associated with hydraulic fracturing. The increasing strain rate increases the breakdown pressure and reduces the fracture productivity due to the increase of fracture tortuosity and the decrease of the fracture aperture.

## 8. Conclusions

The effect of strain rate on tensile fractures was investigated in this study in three different rock types; marlstone, marble, and hornfels. Mineralogical composition and grain size distribution were determined for the three rock types. The crack propagation speed was measured by using a special electrical circuit and the fracture path of the tensile crack was traced under the microscope. The results indicated that:

Taking into account the mineralogical composition and grain size distribution of the three rock types, marlstone has the minimum grain size and it adds the effect of very fine grains on tensile fracturing, especially the effect of weak components such as clay. Marble has the maximum grain size and takes the effect of natural fractures such as intragranular, intergranular cracks, and weak cleavages into account. While hornfels represents the effect of strong minerals on tensile fractures.

Marlstone has the minimum density and the maximum porosity of the three rock types. Moreover, the tensile strength of hornfels is found to be 6 and 7 times greater than that of marble and marlstone, respectively.

By increasing the strain rate from $10^{-5}$ to $10^{-2}$, the $K_{IC}$ in marlstone, marble, and hornfels increases from 0.65 to 1.03, 1.0 to 1.72, and 2.01–3.73 MPa $m^{0.5}$, respectively. In addition, the increment rate of $K_{IC}$ varies according to the rock type such that the increment rate of marlstone, marble, and hornfels is 0.4%, 0.75%, and 1.8%, respectively.

The crack propagation speed is dependent on the strain rate such that by increasing the strain rate from $10^{-5}$ to $10^{-2}$, the crack propagation speed in marlstone and marble increases from 4 to 22 m/s, and in hornfels increases from 35 to about 100 m/s. The results concluded that the hornfels has the maximum increment rate of crack propagation speed (65%), while marlstone and marble have the same increment rate of 18%.

We also found that as the grain size increases, the tortuosity factor increases and so the marlstone has the minimum tortuosity factor. Moreover, under a strain rate of $10^{-5}$, the tortuosity factor of marble is found to be 7.5% and 4.5% greater than that in marlstone and hornfels, respectively. As the strain rate increased from $10^{-5}$ to $10^{-2}$ $S^{-1}$; the tortuosity factor in marlstone, marble, and hornfels increased by 0.5%, 4.8%, and 0.3%, respectively.

The fracture width is affected by the strain rate and it was found that by increasing the strain rate from $10^{-5}$ to $10^{-2}$ in marlstone, marble, and hornfels, the fracture width decreases by 36%, 26%, and 34%, respectively. Therefore, the permeability of tensile cracks decreases.

## Declaration of competing interest

The authors declare that they have no known competing financial interests or personal relationships that could have appeared to influence the work reported in this paper.

## Data availability

Data will be made available on request.

## Acknowledgment

We would like to extend our thanks to Vahid Ghafarinia and Nader Karimi for their efforts in providing us with the necessary equipment to measure the rupture speed. In addition, Azmoneh Foulad Consulting Engineers is acknowledged for permission to use facilities in this company's rock mechanics lab under the supervision of Mohsen Aghababaei and Behzad Nateghpour.

## References

1 Gale JF, Laubach SE, Olson JE, Eichhubl P, Fall A. Natural fractures in shale: a review and new observationsNatural fractures in shale: a review and new observations. *AAPG (Am Assoc Pet Geol) Bull.* 2014;98(11):2165–2216.
2 Li H, Zhao J, Li T. Triaxial compression tests on a granite at different strain rates and confining pressures. *Int J Rock Mech Min.* 1999;36(8):1057–1063.
3 Blanton T. Effect of strain rates from 10-2 to 10 sec-1 in triaxial compression tests on three rocks. *Int J Rock Mech Min Sci.* 1981;18:47–62.
4 Lajtai EZ, Duncan E, Carter B. The effect of strain rate on rock strength. *Rock Mech Rock Eng.* 1991;24(2):99–109.
5 Mahanta B, Tripathy A, Vishal V, Singh T, Ranjith P. Effects of strain rate on fracture toughness and energy release rate of gas shales. *Eng Geol.* 2017;218:39–49.
6 Li H, Zhao J, Li T. Micromechanical modelling of the mechanical properties of a granite under dynamic uniaxial compressive loads. *Int J Rock Mech Min.* 2000;37(6):923–935.
7 Wu Z, Wong LNY. Investigating the effects of micro-defects on the dynamic properties of rock using Numerical Manifold method. *Construct Build Mater.* 2014;72:72–82.
8 Alzo'ubi A. Stability of a rock slope susceptible to seasonal movements. *Int J Geomate.* 2014;6:800–805.
9 Yoffe EH. The moving Griffith crack. *Lond Edinb Dubl Phil Mag.* 1951;42(330):739–750.
10 Yamashita T. Generation of microcracks by dynamic shear rupture and its effects on rupture growth and elastic wave radiation. *Geophys J Int.* 2000;143(2):395–406.
11 Jiang C, Zhao G-F, Khalili N. On crack propagation in brittle material using the distinct lattice spring model. *Int J Solid Struct.* 2017;118:41–57.
12 Ruiz G, Ortiz M, Pandolfi A. Three-dimensional finite-element simulation of the dynamic Brazilian tests on concrete cylinders. *Int J Numer Methods Eng.* 2000;48(7):963–994.
13 Zhou X-P, Wang Y-T. Numerical simulation of crack propagation and coalescence in pre-cracked rock-like Brazilian disks using the non-ordinary state-based peridynamics. *Int J Rock Mech Min.* 2016;89:235–249.
14 Aliha M, Mousavi S, Ghoreishi S. Fracture load prediction under mixed mode I+ II using a stress based method for brittle materials tested with the asymmetric four-point bend specimen. *Theor Appl Fract Mech.* 2019;103, 102249.
15 Ayatollahi M, Shadlou S, Shokrieh M. Mixed mode brittle fracture in epoxy/multi-walled carbon nanotube nanocomposites. *Eng Fract Mech.* 2011;78(14):2620–2632.
16 Aliha M, Hosseinpour GR, Ayatollahi M. Application of cracked triangular specimen subjected to three-point bending for investigating fracture behavior of rock materials. *Rock Mech Rock Eng.* 2013;46(5):1023–1034.
17 Griffith WA, Rosakis A, Pollard DD, Ko CW. Dynamic rupture experiments elucidate tensile crack development during propagating earthquake ruptures. *Geology.* 2009;37(9):795–798.

18 Ngo D, Huang Y, Rosakis A, Griffith W, Pollard D. Off-fault tensile cracks: a link between geological fault observations, lab experiments, and dynamic rupture models. *J Geophys Res Solid*. 2012;117(B1).
19 Mighani S, Sondergeld CH, Rai CS. Observations of tensile fracturing of anisotropic rocks. *SPE J*. 2016;21(4):1289–1301.
20 Zhang J, Kamenov A, Zhu D, Hill A. Measurement of realistic fracture conductivity in the Barnett shale. *J Unconv Oil Gas Resour*. 2015;11:44–52.
21 Zhang J, Ouyang L, Hill AD, Zhu D. Experimental and numerical studies of reduced fracture conductivity due to proppant embedment in shale reservoirs. In: *SPE Annual Technical Conference and Exhibition*. 2014. OnePetro.
22 Lu Z, Yao J, Li L. Experimental study on fluid flow characteristics in orthogonal fracture network. *J China Coal Soc*. 2010;35:555–558.
23 Zhao J, Lee B, Lee T-W, Kim C-G, Shin J-K, Cho J. Flexible dual tcp/udp streaming for h. 264 hd video over wlans. In: *Proceedings of the 7th International Conference on Ubiquitous Information Management and Communication*. 2013:1–9.
24 Pandey VJ, Flottman T, Zwarich NR. Applications of geomechanics to hydraulic fracturing: case studies from coal stimulations. *SPE Prod Oper*. 2017;32(4):404–422.
25 Wen Q, Wang S, Duan X, Li Y, Wang F, Jin X. Experimental investigation of proppant settling in complex hydraulic-natural fracture system in shale reservoirs. *J Nat Gas Sci Eng*. 2016;33:70–80.
26 Abe A, Kim TW, Horne RN. Laboratory hydraulic stimulation experiments to investigate the interaction between newly formed and preexisting fractures. *Int J Rock Mech Min*. 2021;141, 104665.
27 Alneasan M, Behnia M. An experimental investigation on tensile fracturing of brittle rocks by considering the effect of grain size and mineralogical composition. *Int J Rock Mech Min*. 2021;137, 104570.
28 Committee CL. A guide to core logging for rock engineering. *Bull Assoc Eng Geol*. 1978;15(3):295–328.
29 Shoval S. Mineralogical changes upon heating calcitic and dolomitic marl rocks. *Thermochim Acta*. 1988;135:243–252.
30 Feng G, Wang X, Wang M, Kang Y. Experimental investigation of thermal cycling effect on fracture characteristics of granite in a geothermal-energy reservoir. *Eng Fract Mech*. 2020;235, 107180.
31 Shao S, Ranjith P, Wasantha P, Chen B. Experimental and numerical studies on the mechanical behaviour of Australian Strathbogie granite at high temperatures: an application to geothermal energy. *Geothermics*. 2015;54:96–108.
32 Mertoglu O, Simsek S, Basarir N, Paksoy H. Geothermal energy use, country update for Turkey. *Proceedings of the European Geothermal Congress*. 2019:11–14.
33 Cui J, Yuan X, Wu S, Zhang R, Jin S, Li Y. Rock types and reservoir characteristics of Shahejie formation Marl in Shulu Sag, Jizhong Depression, Bohai Bay Basin. *J Earth Sci*. 2021;32(4):986–997.
34 Fu X, Wu J, Shou J, et al. Tight oil reservoir characteristics of lacustrine mixed marlstone in the palaeogene Shahejie formation of Shulu Sag, Bohai Bay Basin. *Oil Gas Geol*. 2019;40(1):78–91.
35 Bieniawski ZT. *Engineering Rock Mass Classifications: A Complete Manual for Engineers and Geologists in Mining, Civil, and Petroleum Engineering*. New York: Wiley; 1989.
36 Bieniawski Z, Hawkes I. Suggested methods for determining tensile strength of rock materials. *Int J Rock Mech Min Sci*. 1978;15(3):99–103.
37 Chen J, Zhou L, Li H, Shen Z, Xia B. Comparison on hydraulic and mechanical responses to the growing loading between both fractures induced by hydraulic fracturing and Brazilian splitting. *Energy Fuels*. 2020;34(9):10933–10946.
38 Mousavi S, Aliha M, Imani D. On the use of edge cracked short bend beam specimen for PMMA fracture toughness testing under mixed-mode I/II. *Polym Test*. 2020;81, 106199.
39 Alneasan M, Behnia M. Strain rate effects on the crack propagation speed under different loading modes (I, II and I/II): experimental investigations. *Eng Fract Mech*. 2021;258, 108118.
40 Alneasan M, Behnia M. Analytical and experimental investigation on the effect of loading rate on the fracture toughness and fracture envelope in brittle rocks. *Theor Appl Fract Mech*. 2022, 103300.
41 Alneasan M, Alzo'ubi AK, Behnia M, Mughieda O. Experimental observations on the effect of thermal treatment on the crack speed and mode i and ii fracture toughness in brittle and ductile rocks. *Theor Appl Fract Mech*. 2022, 103525.
42 Crouch SL, Starfield AM, Rizzo F. Boundary element methods in solid mechanics. *J Appl Mech*. 1983;50:704.
43 Alzo'ubi A. *Modeling Yield Propagation of Jointed Synthetic Rock*. ISRM International Symposium-EUROCK 2016; 2016. OnePetro.
44 Whittaker BN, Singh RN, Sun G. *Rock Fracture Mechanics. Principles, Design and Applications*. 1992.
45 Broberg KB. *Cracks and Fracture*. Amsterdam: Elsevier; 1999.
46 Freund LB. *Dynamic Fracture Mechanics*. Cambridge: Cambridge University Press; 1998.
47 Brown SR. Transport of fluid and electric current through a single fracture. *J Geophys Res Solid*. 1989;94(B7):9429–9438.
48 Li H, Lai B, Liu H-H, Zhang J, Georgi D. Experimental investigation on Brazilian tensile strength of organic-rich gas shale. *SPE J*. 2018;22(1):148–161.
49 Alzo'ubi AK. Effect of strength properties on displacement mag-nitude and fracturing amount inside a large open pit prone to toppling. *J GeoEngin*. 2019;14(2):65–76.
50 Zhang J, Lai B, Liu H-H, Li H, Georgi D. Textural and mineralogical control on tensile strength of Eagle Ford and Manco shales samples. In: *SPE/AAPG/SEG Unconventional Resources Technology Conference*. 2016. OnePetro.
51 Johnson J, Clifton R, Simonson E, Green S. Analysis of fracture of hollow cylindrical and spherical rock specimens subjected to internal pressure with applications to underground nuclear containment. *Terra*. 1973;235, 73-50.
52 Paris PC, Sih GC. *Stress Analysis of Cracks. Fracture Toughness Testing and its Applications*. ASTM International; 1965.
53 Mohamadi A, Behnia M, Alneasan M. Comparison of the classical and fracture mechanics approaches to determine in situ stress/hydrofracturing method. *Bull Eng Geol Environ*. 2021;80(5):3833–3851.
54 Zhuang L, Kim KY, Jung SG, Diaz M, Min K-B. Effect of water infiltration, injection rate and anisotropy on hydraulic fracturing behavior of granite. *Rock Mech Rock Eng*. 2019;52(2):575–589.
55 Morgan S, Li B, Einstein H. *Effect of Injection Rate on Hydraulic Fracturing of Opalinus Clay Shale. 51st US Rock Mechanics/Geomechanics Symposium*. OnePetro; 2017.
56 Ha SJ, Yun TS, Kim KY, Jung SG. Experimental study of pumping rate effect on hydraulic fracturing of cement paste and mortar. *Rock Mech Rock Eng*. 2017;50(11): 3115–3119.
57 Tsang Y. The effect of tortuosity on fluid flow through a single fracture. *Water Resour Res*. 1984;20(9):1209–1215.
58 Lespinasse M, Sausse J. Quantification of fluid flow: hydro-mechanical behaviour of different natural rough fractures. *J Geochem Explor*. 2000;69:483–486.